Reaction Chemistry & Engineering

COMMUNICATION

View Article Online
View Journal | View Issue

Cite this: *React. Chem. Eng.*, 2019, 4, 663

Received 3rd October 2018,
Accepted 4th December 2018

DOI: 10.1039/c8re00241j

rsc.li/reaction-engineering

Continuous synthesis of Zn_2Al–CO_3 layered double hydroxides: a comparison of bench, pilot and industrial scale syntheses†

I. Clark, [ab] R. L. Gomes, [b] C. Crawshaw,[c] L. Neve,[c] R. Lodge, [d] M. Fay, [d] C. Winkler,[e] M. Hull[e] and E. Lester *[a]

Zn_2Al–CO_3 was produced continuously at bench (g h^{-1}), pilot (100s g h^{-1}) and industrial scale (10s kg h^{-1}). Crystal domain length and BET surface area were similar at all three scales although there was a small increase at pilot scale. Platelet size increased from 120 nm at bench to 177 nm and 165 nm at pilot scale and industrial scale, respectively. Overall this paper shows that the increase in scale by almost 2000× does not impact on the overall product quality which is an excellent indicator that continuous hydrothermal synthesis is a route for nanomaterials synthesis.

Layered double hydroxides (LDHs) are a type of synthetic anionic clay that form from layers of hydroxides of bi-valent and tri-valent metal ions. The layers are held together through electrostatic attractions with interlayer anions. Hydrotalcite is a naturally forming LDH composed of Mg^{2+} and Al^{3+} metal ions with CO_3^{2-} as the interlayer anion.[1,2] However Mg^{2+} and Al^{3+} can be substituted with an array of cations (Zn^{2+}, Co^{2+}, Cr^{3+}) and likewise CO_3^{2-} can be alternated with many other anions (NO_3^-, Cl^-).[3] All LDHs follow the same structural formula – $[M^{II}_xM^{III}_{1-x}(OH)_2](A^{n-})_{x/n}{\cdot}zH_2O$, M^{II} and M^{III} represent metal ions and A^{n-} represents the interlayer anion.[1,2] LDHs are most typically produced through a co-precipitation route.[4–6] More recently there have been attempts to blend continuous hydrothermal synthesis – a method more commonly associated with supercritical synthesis of metal oxide nanomaterials – with the synthesis of LDHs. Wang *et al.* first utilised continuous hydrothermal synthesis (CHS) using a tube-in-tube counter current reactor design to produce Mg_2Al–CO_3 and Ca_2Al–NO_3 under sub- and supercritical water conditions. Under supercritical conditions AlOOH begins to form, resulting in a less pure product. It was also noted that control of temperature and pressure within the system provided some amount of control over crystal size.[9] Clark *et al.* used a similar reactor set up to further investigate reaction variables in CHS, examining the effect of low temperature synthesis for tuneable control of crystal domain length. Excessive NaOH content resulted in $Ca(OH)_2$ impurities during product formation.[10] Zn based LDHs have been investigated for use in adsorption and in photocatalytic applications. ZnAl–CO_3 was compared with MgAl–CO_3 and NiAl–CO_3 for adsorption of Cr(VI), with the ZnAl–CO_3 material exhibiting a larger surface area and uptake capacity.[11] Calcined ZnAl LDHs have also been investigated for phosphorus recovery.[12] Cheng *et al.* found that calcination impacts on adsorption capacity and material characteristics, such as surface area, as calcination breaks down the LDH crystal structure and allows to form mixed metal oxides.[12] ZnAl LDHs have been compared against ZnTi type LDHs, in the case of degradation of organic dyes.[7,8] The structural properties of the ZnAl material yielded better degradation results than ZnTi LDHs despite a larger band gap.[13] The aim of this work was to investigate how scaling synthesis from bench scale synthesis to pilot scale to industrial scale impacted the structural and crystal characteristics of the Zn_2Al–CO_3 layered double hydroxide.

Synthesis was carried out in three separate reactor systems. Bench scale synthesis followed a similar method to that published by Clark *et al.*[10] Synthesis was carried out in a

[a] *Advanced Materials Research Group, Faculty of Engineering, University of Nottingham, Nottingham, NG7 2RD, UK. E-mail: Edward.lester@nottingham.ac.uk*
[b] *Food, Water, Waste Research Group, Faculty of Engineering, University of Nottingham, Nottingham, NG7 2RD, UK*
[c] *Promethean Particles Ltd, 1-3 Genesis Park, Midland Way, NG7 3EF, Nottingham, UK*
[d] *Nanoscale and Microscale Research Centre, The University of Nottingham, Nottingham, NG7 2RD, UK*
[e] *Nanoscale Characterization and Fabrication Laboratory, Virginia Tech, 1991 Kraft Drive Blacksburg, VA 24061, USA*

† Electronic supplementary information (ESI) available. See DOI: 10.1039/c8re00241j

Table 1 Synthesis scale and comparison between flowrate, Reynolds number and space–time yield (STY)

Scale	Flowrate/L h^{-1}	STY/kg^{-1} L^{-1} h^{-1}
Bench	1.8	6.3
Pilot	36	5.2
Industrial	1050	157.3

Table 2 Crystal domain length (CDL) of LDH materials

Sample	CDL ⟨003⟩/nm	CDL ⟨110⟩/nm
B-LDH	18 ± 0	39 ± 1
P-LDH	26 ± 0	50 ± 4
I-LDH	19 ± 0	31 ± 2

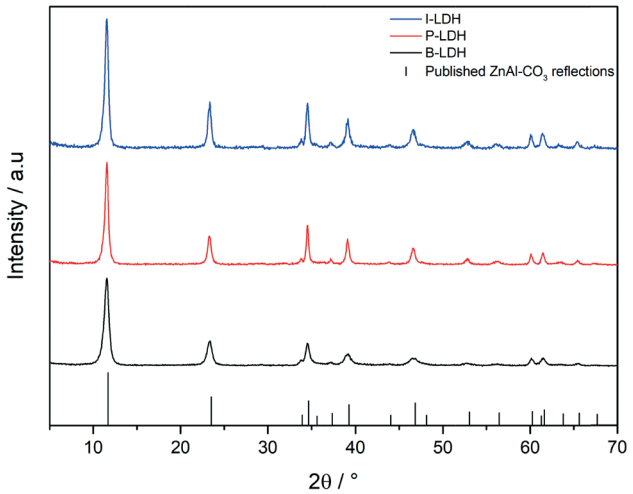

Fig. 1 XRD diffractogram for bench (B-LDH), pilot (P-LDH) and industrial (I-LDH) scale synthesis. Published $ZnAl–CO_3$ reflections from Perez *et al.*[16]

pipe-in-pipe, counter-current flow reactor where a solution of mixed metal salts was flowed up into the reactor, while a solution of NaOH and Na_2CO_3 was pumped down into the reactor, mixing of the fluids occurs at the outlet of the inner tube, where the base solution flows into the outer reactor tubing. Bench scale synthesised $Zn_2Al–CO_3$ is herein referred to as B-LDH, pilot samples are indicated by P-LDH and industrial scale LDH samples are indicated by I-LDH (Details of synthesis processes can be found in ESI†).

Increases in synthesis scale between bench, pilot and industrial synthesis were compared to establish yield changes between different flow rates, while maintaining precursor concentration between all three scales. The increase in reactor size between bench and pilot scale reactors is not matched by the increase in reaction flowrates, with an increase in flow rate of a factor of twenty. The increase in scale from pilot from industrial utilises a significantly increased throughflow, and as a result the space time yield is increased significantly (Table 1).

$Zn_2Al–CO_3$ exhibits hexagonal crystal symmetry in a rhombohedral setting with space from $R\bar{3}m$ (Fig. 1). Lattice parameters for B-LDH were 0.30 nm and 2.29 nm for a and c respectively.[2] Lattice parameters for P-LDH were 0.31 nm for a and 2.29 nm for c. Estimation of crystal domain length (CDL) calculated using the full width at half maximum (FWHM) of the (003) and (110) reflections. The data in Table 2 indicates a marginal increase in CDL size in the scaling of synthesis from 30 mL min^{-1} to 600 mL min^{-1}. This phenomenon has been illustrated previously in the scaling continuous hydrothermal synthesis of ceramic nanoparticles,[14] although to a lesser extent. However, increasing scale to industrial synthesis at 1050 L h^{-1}, resulted in a CDL that is comparable to the B-LDH sample in the ⟨003⟩ plane. The cause of increased crystal size between P-LDH and B-LDH was mostly likely due to the post processing period where the pilot scale particles were allowed to settle, in order to reduce the overall volume liquid product, before being washed. During the prolonged period for settling, some degree of Ostwald ripening may occur or continued precipitation of any residual precursor in the reactor effluent.

SEM and TEM micrographs (Fig. 2 and 3) of the scaled materials show distinct platelet like particles. The stacking arrangement of platelets in B-LDH shows a high degree of face–face stacking and agglomeration in the SEM micrograph (Fig. 2a), this is a familiar characteristic of LDH materials and can be seen in a variety of different types.[10,15] On the other hand, the P-LDH sample exhibits a greater degree of edge face stacking as seen in the more open flower-like micro-structure depicted in the SEM micrograph (Fig. 2b) and the TEM micrograph (Fig. 3b). The microstructure of the I-LDH sample in Fig. 2c is similar to the P-LDH sample, with an open structure and edge-face agglomeration. The particles displayed in Fig. 3c exhibit a regular hexagonal shape and agglomerate together similarly to particles in the B-LDH and P-LDH samples.

Particle size distribution of the B-LDH platelets was 120 ± 53 nm, while the increase in scale shows an increase in particle diameter to 177 ± 74 nm at pilot scale and 165 ± 55 nm at industrial scale (Fig. 4). The platelet diameter calculated image analysis of TEM micrographs is larger than the CDL due to the fact that the CDL was only a measure of the repeating units and

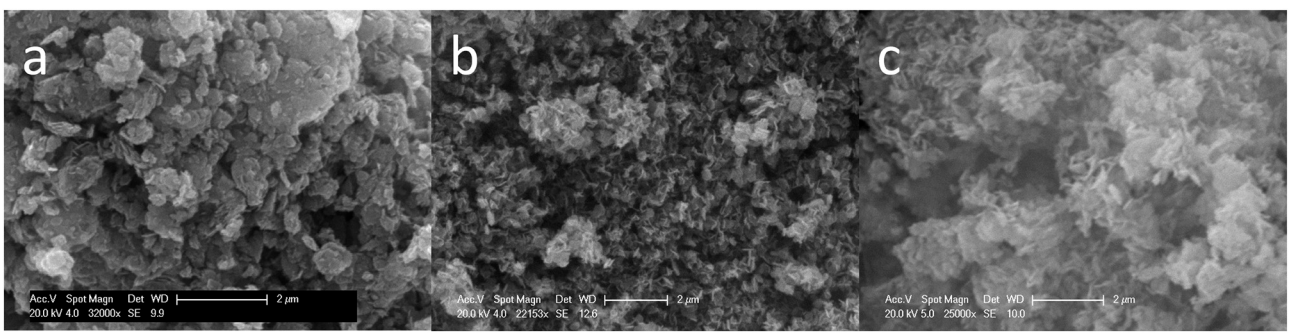

Fig. 2 SEM images of bench (a), pilot (b) and industrial (c) scale LDH samples.

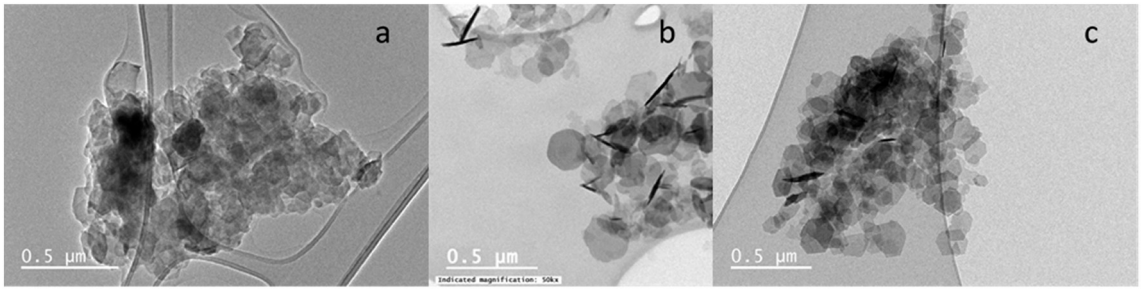

Fig. 3 TEM images of bench (a), pilot (b) and industrial (c) scale LDH samples.

cannot account for faults in the crystal structure and amorphous regions in the material. The coefficient of variance decreases with increased scale, indicating that despite an increase in the deviation of the platelet diameter, in relation to the mean the size distribution decreases with scale.

The I-LDH sample exhibited a mean platelet diameter 12 nm smaller than the P-LDH sample, indicating that with increased scale and flow the particle size increases, however with the more turbulent flow within the system maintains a narrow size distribution (Table 3).

All LDH samples exhibit type-IV isotherms with H3 hysteresis. This indicates the materials are mesoporous, consisting of loose agglomerates of lamellar particles.[17] The pore size distribution suggests that there is a high concentration of pores close to the boundary between mesopores (2–50 nm) and macropores (>50 nm),[17] indicating that macrospores are present in the agglomerates of finer particles. The data in Table 4 shows that surface area (S_{BET}) and average pore diameter were both larger in the bench scale sample when compared with the pilot scale sample. The more open structure of P-LDH agglomerates led to more accessible small mesopores (≈2 nm).[17] There is a greater proportion of micropore volume in the P-LDH sample compared with a greater proportion of mid and high range mesopore volume (10–50 nm) in the B-LDH and I-LDH samples. The total pore volume is greater in the B-LDH sample due to the smaller contribution of mesopore volume in the P-LDH compared with the B-LDH sample, thus despite a larger pore diameter the volume of mesopores in the B-LDH sample contributes to an increased S_{BET}. The S_{BET} of the I-LDH sample is 64.1 ± 0.2 m^2 g^{-1}, which is greater than both the B-LDH and P-LDH samples. This is primarily due to the greater number of mesopores around 40–50 nm (Fig. 5).

The difference in Zn_2Al–CO_3 produced by continuous synthesis at bench, pilot and industrial scale has been investigated across a range of characteristics. The crystal structure of the materials remains similar with small differences in domain length in both ⟨003⟩ and ⟨110⟩ planes. B-LDH shows smaller CDL in both crystal planes compared to P-LDH with CDL in the ⟨003⟩ plane at 18 nm and 26 nm for B-LDH and P-LDH respectively while the CDL in the ⟨110⟩ plane is larger for both materials and P-LDH again displaying the longer domain length at 50 nm compared with 39 nm for B-LDH. The CDL of the industrial scale sample is closer in scale to the B-LDH sample indicating that the increased CDL observed in the P-LDH sample is primarily due to the post settling period after pilot scale synthesis. Platelet size determined from TEM micrographs shows that the P-LDH average platelet size is 177 nm while the B-LDH is 120 nm, while the average particle diameter of the I-LDH sample was 166 nm. The M^{II}/M^{III} ratio of both bench and pilot scale samples was close to the theoretical ratio of 2, while the Zn/Al ratio of the I-LDH sample was 2.8 (data available in ESI†). This indicates that there was an imbalance in the co-precipitation of the metal hydroxides and $Zn(OH)_2$ was produced preferentially under the industrial scale conditions. Surface area values are similar and averaged out at 58m^2 g^{-1} although the industrial scale gave the highest value at 64 m^2 g^{-1}. P-LDH particles probably exhibited a smaller S_{BET} as a result of being larger with a decreased

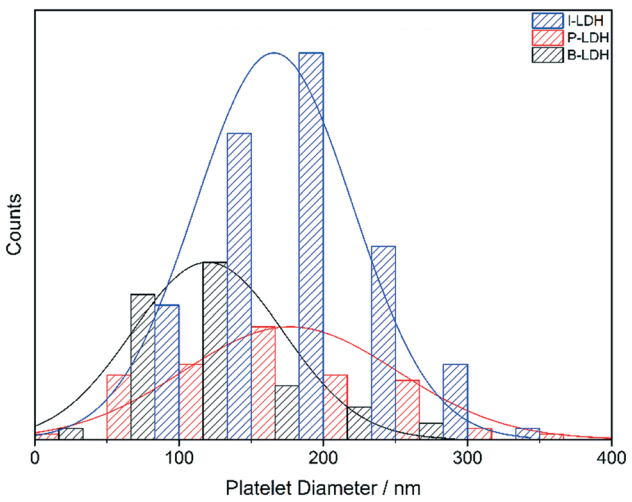

Fig. 4 Particle size distribution of bench (B-LDH), pilot (P-LDH) and industrial (I-LDH) scale LDH samples.

Table 3 Synthesis scale and comparison between flowrate, Reynolds number and space–time yield (STY)

Scale	Flowrate/L h^{-1}	Reynolds number	Flow	STY/kg^{-1} L^{-1} h^{-1}
Bench	1.8	68	Laminar	6.3
Pilot	36	310	Laminar	5.2
Industrial	1050	9050	Turbulent	157.3

Table 4 Specific surface area (S_{BET}), pore diameter and volume

Sample	S_{BET}/m^2 g^{-1}	Pore diameter/nm	Pore volume/cm^3 g^{-1}
B-LDH	58.0 ± 0.1	19.1	0.3
P-LDH	50.1 ± 0.2	15.3	0.2
I-LDH	64.1 ± 0.2	19.7	0.4

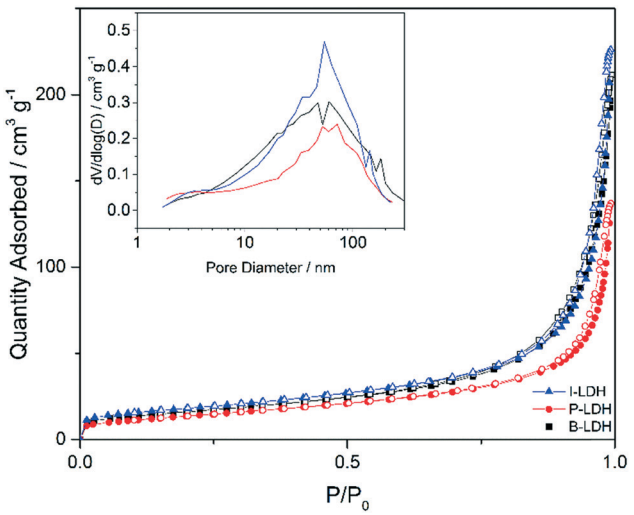

Fig. 5 Nitrogen adsorption isotherms for bench and pilot scale samples (inset – pore size distribution).

mesopore volume, compared to the B-LDH and I-LDH particles. The CDL and size distribution appear to have an impact on surface area of the sample and the changes with increased scale result in greater surface area and smaller crystallite characteristics.

Conflicts of interest

There are no conflicts to declare.

Acknowledgements

This work was supported by the Engineering and Physical Sciences Research Council [grant number EP/M506588/1] as part of the Doctoral Training Partnerships – University of Nottingham. This work was part funded by the European Union's Seventh Framework Programme (FP7/2007–2013), grant agreement no. FP7-NMP4-LA-2012-280983, SHYMAN. Our thanks to the staff at Promethean Particles Ltd for assistance and guidance throughout.

Notes and references

1 F. Cavani, F. Trifiro and A. Vaccari, *Catal. Today*, 1991, **11**, 173–301.
2 S. M. Auerbach, K. A. Carrado and P. K. Dutta, *Handbook of layered materials*, M. Dekker, New York, 2004.
3 R. Xu, W. Pang and Q. Huo, *Mod. Inorg. Synth. Chem.*, 2011, 1–590.
4 S. Miyata, T. Kumura, H. Hattori and K. Tanabe, *Nippon Kagaku Zasshi*, 1971, **92**, 514–519.
5 S. Miyata and A. Okada, *Clays Clay Miner.*, 1977, **25**, 14–18.
6 S. Miyata, *Clays Clay Miner.*, 1980, **28**, 50–56.
7 X. R. Wang, P. X. Wu, Z. J. Huang, N. W. Zhu, J. H. Wu, P. Li and Z. Dang, *Appl. Clay Sci.*, 2014, **95**, 95–103.
8 S. J. Xia, F. X. Liu, Z. M. Ni, W. Shi, J. L. Xue and P. P. Qian, *Appl. Catal., B*, 2014, **144**, 570–579.
9 Q. Wang, S. Tang, E. Lester and D. O'Hare, *Nanoscale*, 2013, **5**, 114–117.
10 I. Clark, P. W. Dunne, R. L. Gomes and E. Lester, *J. Colloid Interface Sci.*, 2017, **504**, 492–499.
11 W. W. Wang, J. B. Zhou, G. Achari, J. G. Yu and W. Q. Cai, *Colloids Surf., A*, 2014, **457**, 33–40.
12 X. Cheng, X. Huang, X. Wang and D. Sun, *J. Hazard. Mater.*, 2010, **177**(1–3), 516–523.
13 S. J. Xia, F. X. Liu, Z. M. Ni, J. L. Xue and P. P. Qian, *J. Colloid Interface Sci.*, 2013, **405**, 195–200.
14 P. W. Dunne, C. L. Starkey, A. S. Munn, S. V. Y. Tang, O. Luebben, I. Shvets, A. G. Ryder, Y. Casamayou-Boucau, L. Morrison and E. H. Lester, *Chem. Eng. J.*, 2016, **289**, 433–441.
15 M. S. Yang, O. McDermott, J. C. Buffet and D. O'Hare, *RSC Adv.*, 2014, **4**, 51676–51682.
16 M. R. Perez, I. Crespo, M. A. Ulibarri, C. Barriga, V. Rives and J. M. Fernandez, *Mater. Chem. Phys.*, 2012, **132**, 375–386.
17 M. Thommes, K. Kaneko, A. V. Neimark, J. P. Olivier, F. Rodriguez-Reinoso, J. Rouquerol and K. S. W. Sing, *Pure Appl. Chem.*, 2015, **87**, 1051–1069.